A baseline closure concept for simulating bubbly flow with phase change: interfacial heat transfer coefficient

Liao, Y.; Krepper, E.; Lucas, D.;

Originally published:

April 2019

Nuclear Engineering and Design 348(2019), 1-13

DOI: https://doi.org/10.1016/j.nucengdes.2019.04.007

Perma-Link to Publication Repository of HZDR:

https://www.hzdr.de/publications/Publ-27711

A baseline closure concept for simulating bubbly flow with phase change: A mechanistic model for interphase heat transfer coefficient

Y. Liao*, E. Krepper, D. Lucas

Helmholtz-Zentrum Dresden – Rossendorf, Germany, Bautzner Landstr. 400, 01328 Dresden, Germany

y.liao@hzdr.de

Abstract In line with the best practice guidelines for computational fluid dynamics in nuclear reactor safety, Helmholtz-Zentrum Dresden – Rossendorf proposed an Euler-Euler baseline closure concept some years ago. The consideration is that simulations with a fixed set of closures instead of case by case tuning may help to identify model inadequacy and facilitate further improvement. Currently, the baseline model concerns interphase momentum and turbulence exchange as well as bubble coalescence and breakup. It has been tested for a wide range of isothermal applications with different geometrical configurations and material systems. In the present work, the baseline model is extended to non-isothermal flows by including a mechanistic model for the computation of overall interphase heat transfer coefficient. The extended baseline model is validated for both bubble-growing in superheated liquid and -condensing in sub-cooled liquid. The baseline model proposal is independent on the use of a certain CFD code. The presented simulation is carried out with the commercial software ANSYS CFX by employing the best practice guidelines. The simulated liquid temperature, gas volume fraction, vapor bubble size and velocity are compared with the measured ones. The effectivity of the model is demonstrated by a general good agreement.

Keywords: Baseline model; Best practice guidelines; CFD; Interphase heat transfer coefficient; Two-fluid model

1. INTRODUCTION

Actual 1D system codes are accepted as a tool for new reactor licensing and reactor safety analysis. However in lots of cases 3D phenomena play an important role and CFD methods are recommended. To obtain reliable results best-practice guidelines (BPG) are necessary and important with respect to model selection, geometry model, grid, initial and boundary conditions, material properties, simulation, error quantification, uncertainty analysis as well as documentation. For this purpose a number of useful documents such as Scheuerer et al. (2005) and Mahaffy et al. (2007) came out and provide practical guidance for application of single phase CFD to the analysis of nuclear reactor safety. Model selection is the first step and also the most difficult one especially in case of complex multiphase flow with interfacial mass, momentum, energy, turbulence exchanges, since a common consensus on the closures is still missing even for the simple example of isothermal monodisperse flows. Therefore, BPG for the application of multiphase CFD are still not available, and it is often the case that a test case is investigated by different researchers with different model setups, but all are able to obtain a good agreement with the measurements after some kind of tuning. The situation is quite dangerous in reactor safety analysis, where usually no experimental data as a target are available and the predictability of models is of special importance. Furthermore, the uncertainty and

* Corresponding author: Tel. +49 351 2602389; Email: y.liao@hzdr.de

inconsistence related to model selection largely retards the understanding of the physical phenomena and the further development of the models.

To improve the situation Helmholtz-Zentrum Dresden – Rossendorf (HZDR) recently proposed a baseline model concept (Lucas et al, 2016; Liao et al, 2018a) for the Euler-Euler approach, which is most frequently adopted and often the only feasible one for multiphase flow scenarios in nuclear safety analysis. The goal of the concept is to develop mechanistic closures that represent local phenomena and BPG for application of multiphase CFD to the analysis of dispersed and stratified flows. Currently, it contains four steps: model specification, simulation, evaluation and development. Firstly, a common basis is established by fixing a set of most physically-based closures as well as their constants. They are applied to simulate a variety of flow configurations, e.g. bubbly flow in vertical, horizontal and inclined tubes, cylindrical and rectangular columns or airlift reactors and stirred tanks. Best-practice guidelines regarding geometry model, grid, initial and boundary conditions as well as material properties are employed in the simulations. Subsequently, the most severe deviations of the results and shortcomings of the models are identified via a systematic evaluation process with consideration of measurement and numerical errors. Local phenomena that are not or inappropriately represented are found out, and suitable laboratory or numerical experiments (direct numerical simulation) are designed and carried out to provide in-depth understanding. As a result a better sub-model is figured out based on the new knowledge and hypotheses.

The complexity of non-isothermal flows is increased vastly by the interphase heat transfer and its coupling with the mass and momentum transfer. A reliable phase change model and heat transfer coefficient is the key in modelling such kind of flows with the Euler-Euler approach. There are a variety of correlations for the interphase heat transfer coefficient, which take into account the effect of conduction, convection and turbulence partially or totally, but mostly in a pure empirical way. Reviews were given e.g. by Mathpati and Joshi (2007) and Liao and Lucas (2018b). A thorough evaluation and conclusive guideline on the suitability of these models is nevertheless still missing. The present work attempts to apply a unified interfacial heat transfer model for numerical simulation of the thermal phase change in condensation and evaporation. It is a step of extending the baseline concept for simulating bubbly flow with phase change. The remainder of the paper is organized as follows. A thorough description of the mathematical model applied for poly-dispersed bubbly flow with phase change is given in Section 2, and detailed information about the relations and theories available for the calculation of interfacial heat transfer coefficient is given separately in Section 3. The simulation setup and results as well as their comparison to the experimental data are presented in Section 4. Finally, a short conclusion and outlook for future work ends the paper.

2. NUMERICAL MODELS FOR PHASE CHANGE

The CFD simulation of gas-liquid bubbly flows with phase change is based on the CFX-18 multi-fluid Euler-Euler approach. Regarding the liquid phase as continuum and the gaseous phase as disperse phase, the ensemble-averaged mass, momentum and energy transport equations for both phases read:

Continuous phase

$$\frac{\partial}{\partial t}\left(\alpha_{\mathrm{l}}\rho_{\mathrm{l}}\right)+\nabla\cdot\left(\alpha_{\mathrm{l}}\rho_{\mathrm{l}}\vec{U}_{\mathrm{l}}\right)=S_{\mathrm{lg}}, \tag{1}$$

$$\frac{\partial}{\partial t}\left(\alpha_{\mathrm{l}}\rho_{\mathrm{l}}\vec{U}_{l}\right)+\nabla\cdot\left(\alpha_{\mathrm{l}}\rho_{\mathrm{l}}\vec{U}_{\mathrm{l}}\vec{U}_{\mathrm{l}}\right)=-\alpha_{\mathrm{l}}\nabla p+\nabla\cdot\left(\alpha_{\mathrm{l}}\vec{\tau}_{\mathrm{l}}\right)+\alpha_{\mathrm{l}}\rho_{\mathrm{l}}\vec{g}+\vec{F}_{\mathrm{lg}}+\vec{S}_{\mathrm{M,\,lg}}\ , \tag{2}$$

$$\frac{\partial}{\partial t}\left(\alpha_{\mathrm{l}}\rho_{\mathrm{l}}\left(H_{\mathrm{tot,\,l}}-\frac{p}{\rho_{\mathrm{l}}}\right)\right)+\nabla\cdot\left(\alpha_{\mathrm{l}}\rho_{\mathrm{l}}\vec{U}_{\mathrm{l}}H_{\mathrm{tot,\,l}}\right)=\nabla\cdot\alpha_{\mathrm{l}}\left(\lambda_{\mathrm{l}}\nabla T_{\mathrm{l}}+\frac{\mu_{\mathrm{t,\,l}}}{\mathrm{Pr}_{\mathrm{t}}}\nabla H_{l}\right)+q_{\mathrm{lg}}+S_{\mathrm{E,\,lg}}\ . \tag{3}$$

Dispersed phase

$$\frac{\partial}{\partial t}\left(\alpha_{\mathrm{g}}\rho_{\mathrm{g}}\right)+\nabla\cdot\left(\alpha_{\mathrm{g}}\rho_{\mathrm{g}}\vec{U}_{\mathrm{g}}\right)=-S_{\mathrm{lg}}, \tag{4}$$

$$\frac{\partial}{\partial t}\left(\alpha_{\mathrm{g}}\rho_{\mathrm{g}}\vec{U}_{\mathrm{g}}\right)+\nabla\cdot\left(\alpha_{\mathrm{g}}\rho_{\mathrm{g}}\vec{U}_{\mathrm{g}}\vec{U}_{\mathrm{g}}\right)=-\alpha_{\mathrm{g}}\nabla p+\nabla\cdot\left(\alpha_{\mathrm{g}}\vec{\tau}_{\mathrm{g}}\right)+\alpha_{\mathrm{g}}\rho_{\mathrm{g}}\vec{g}-\vec{F}_{\mathrm{lg}}-\vec{S}_{\mathrm{M,\,lg}}. \tag{5}$$

The source terms, S_{lg}, $\vec{S}_{\mathrm{M,\,lg}}$, $S_{\mathrm{E,\,lg}}$, represent the volumetric mass transfer rate from gas to liquid due to phase change, the secondary sources of momentum and energy due to mass transfer, respectively. They are given as

$$S_{\mathrm{lg}}=\Gamma^{+}_{\mathrm{lg}}-\Gamma^{+}_{\mathrm{gl}}, \tag{6}$$

$$\vec{S}_{\mathrm{M,\,lg}}=\Gamma^{+}_{\mathrm{lg}}\vec{U}_{\mathrm{g}}-\Gamma^{+}_{\mathrm{gl}}\vec{U}_{\mathrm{l}}, \tag{7}$$

$$S_{\mathrm{E,lg}}=\Gamma^{+}_{\mathrm{lg}}H_{\mathrm{tot,\,ls}}-\Gamma^{+}_{\mathrm{gl}}H_{\mathrm{tot,\,l}}, \tag{8}$$

where Γ^{+}_{lg}, Γ^{+}_{gl} means the positive flux from gas to liquid and liquid to gas, respectively. For example, in case of evaporation, i.e. $\Gamma_{\mathrm{lg}}<0$, Γ^{+}_{lg} is set to zero while $\Gamma^{+}_{\mathrm{gl}}=-\Gamma_{\mathrm{lg}}$ is a positive value, and thus $S_{\mathrm{lg}}=-\Gamma^{+}_{\mathrm{gl}}=\Gamma_{\mathrm{lg}}$, while in the opposite case (condensation), $S_{\mathrm{lg}}=\Gamma^{+}_{\mathrm{lg}}=\Gamma_{\mathrm{lg}}$. The explanation of the interfacial mass transfer rate Γ_{lg} as well as its relation to the interphase heat flux q_{lg} is given in Section 2.1. For the computation of the momentum carried by the mass transferred across the interface, a so-called upwind algorithm is employed. That means that the evaporated mass possesses the velocity of the liquid phase while the condensed mass has that of the gas phase. The calculation of the secondary heat flux $S_{\mathrm{E,lg}}$ is modified to take account of the discontinuity in static enthalpy due to latent heat between the two phases. It is assumed that the bulk fluid enthalpy is carried out of the outgoing phase while the saturation enthalpy is carried into the incoming phase (Ansys, 2018). In addition, the gaseous phase and the gas-liquid interface is assumed to always have the saturation condition. The symbol $H_{\mathrm{tot,ls}}$ in Eq. (8) represents the saturation liquid enthalpy. The term $\vec{F}_{\mathrm{lg}}$ in Eq. (2) and Eq. (4) represents the interfacial momentum transfer due to forces acting on the liquid phase by the bubbles. Drag and non-drag, namely lift, turbulent dispersion, virtual mass and wall lubrication forces are considered in this work. A detailed description of these forces and corresponding models as well as two-phase turbulence modelling with the consideration of bubble-induced turbulence is presented in Liao et al. (2015) and Liao et al. (2019). Note that additional source terms due to nucleation and wall heat flux appear in the equations in case of boiling flows (Janet et al., 2015). For brevity, details of these models are not described here, since they can be found in abundant previous work.

2.1 Interfacial heat and mass transfer

Mass transfer in the thermal phase change process is induced by interphase heat transfer. If the sensible heat flux to the gaseous phase from the interface is neglected as discussed above, the mass transfer rate between the gas and liquid phases is obtained from the sensible heat flux from the interface to the liquid phase q_{lg}

$$q_{lg} = h_l \left(T_{sat} - T_l\right) A_{lg}, \tag{9a}$$

$$\Gamma_{lg} = \frac{q_{lg}}{H_{tot,gi} - H_{tot,li}}, \tag{9b}$$

where h_l is the interphase heat transfer coefficient on the liquid side. A separate discussion on available models and relations is given in section 3. $H_{tot,gi}$ and $H_{tot,li}$ represent interfacial values of total enthalpy carried into and out of the phases due to phase change. $H_{tot,li} = H_{tot,ls}$ if $\Gamma_{lg} > 0$ and $H_{tot,li} = H_{tot,l}$ if $\Gamma_{lg} < 0$, while $H_{tot,gi}$ is always equal to the saturation steam enthalpy.

The interfacial area density A_{lg} is determined by applying the particle model implemented in CFX solver (Ansys, 2018). For rigid spherical bubbles, the relation of area density to gas volume fraction and the Sauter mean bubble diameter is given by:

$$A_{lg} = \frac{6\alpha_g}{d_b}. \tag{10}$$

The simple particle model is modified for high gas volume fractions, where large deformable bubbles are present and the assumption of spherical bubbles is not valid any more. The modifications reflect the reduction of interfacial area density as the gas volume fraction increases and the bubble deforms. The limit is $A_{lg} = 0$ at $\alpha_g = 1$. On the other hand, the lower limit of gas volume fraction is clipped to a minimum value to ensure that the area density does not go exactly to zero and avoid numerical instabilities. Finally, the expression for the area density becomes:

$$A_{lg} = \frac{6\tilde{\alpha}_g}{d_b} \tag{11}$$

with

$$\tilde{\alpha}_g = \begin{cases} \max\left(\alpha_g, \alpha_{min}\right) & \text{if } \left(\alpha_g < \alpha_{max}\right) \\ \max\left(\dfrac{1-\alpha_g}{1-\alpha_{max}}\alpha_{max}, \alpha_{min}\right) & \text{if } \left(\alpha_g > \alpha_{max}\right) \end{cases} \tag{12}$$

The values of 0.8 and 10^{-7} are used for α_{max} and α_{min}, respectively. For the computation of non-drag forces, the solver modifies the interfacial area density further in two ways. Firstly, the area density is permitted to go to zero by setting α_{min} to zero. In addition, the area density is reduced more aggressively as the gas volume fraction increases by multiplying Eq. (11) with a reduction factor

$$f = \left(\frac{1-\alpha_g}{1-\alpha_g'} \right)^n , \tag{13}$$

where

$$\alpha_g' = \begin{cases} \alpha_g & \text{if } \alpha_g \le 0.25 \\ 0.393855 - 0.57142\alpha_g & \text{if } 0.25 < \alpha_g \le 0.6 \\ 0.05 & \text{otherwise} \end{cases} . \tag{14}$$

The area density reduction exponent n is set to 5.

2.2 Inhomogeneous MUSIG

Considering the fact that bubble size changes continuously during evaporation and condensation, a population balance model (inhomogeneous MUSIG) instead of mono-disperse assumption is adopted for the description of bubble size distribution. The heat transfer is calculated based on the Sauter mean diameter of the gas phases (or velocity groups) instead of the size of each group. The inhomogeneous MUSIG model assumes a spectrum of bubble size, which is discretized into a number of groups, e.g. i=1…ΣM_J in Fig. 1, and J represents the velocity group number.

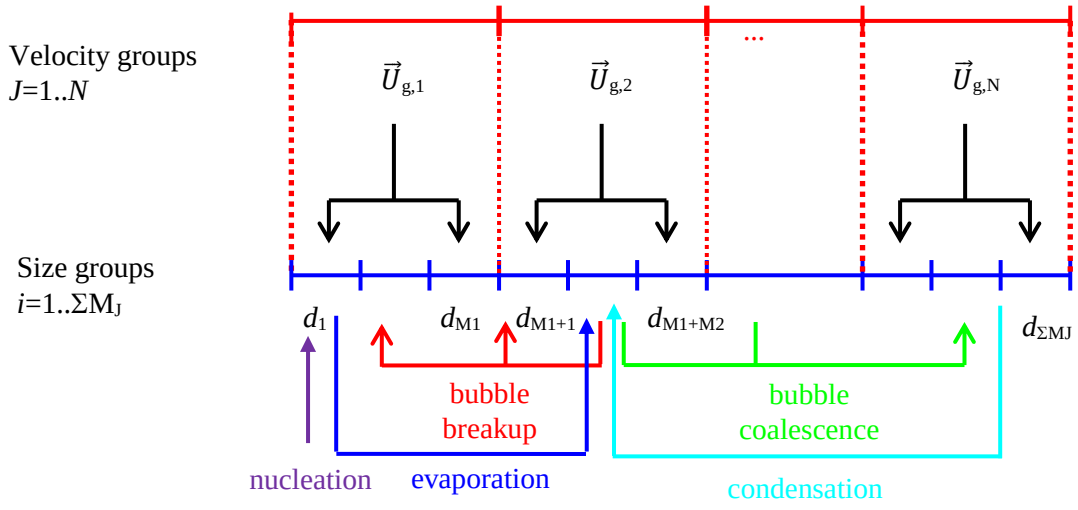

Fig. 1. General schema of the Inhomogeneous MUSIG model

It provides the opportunity to capture the change of bubble size distribution and the transfer between the size groups caused by condensation, evaporation, coalescence, breakup, and so on. In addition, it is possible to take into account the dependence of velocity on bubble size by assuming several velocity groups (N>1). For simplicity, the equations given below are based on one velocity group, i.e. N=1. Sufficient information can be found in our previous work with regards to the formulations for multi velocity groups, e.g. Krepper et al. (2008), Liao et al. (2015) and Liao and Lucas (2016). For the test case of condensing steam-water flow that presented below in Section 4.2, 2 velocity groups are defined. The idea of using 2 velocity groups is to reproduce the sign change of the lift coefficient C_L during the momentum exchange. The boundary of bubble size between Gas1 and Gas2 is in accordance to the transition point in C_L, which is referred to as critical bubble size d_{crit}, see Fig. 2. The value of d_{crit} depends strongly on physical properties and bubble shapes. If the bubble shape can be approximated by using the

Wellek (1966) correlation, for air-water flows under normal conditions d_{crit} is known to be around 6 mm according to Tomiyama et al. (2002), while for steam-water under 20 bar it decreases to 4.4 mm. It should be stressed that the shape of bubbles and thus the d_{crit} in practical systems may deviate largely from the prediction, since it depends on liquid impurity sensitively. The bubbles are equally divided into a number of size groups with a width of 1 mm, which is a commonly used value, e.g. in Yeoh et al. (2012) and Krepper et al. (2009). In addition, for bubbly flow in vertical pipe Krepper et al. (2005) showed that the difference between the calculations was small as the bin width was reduced from 1.5 mm to 0.25 mm.

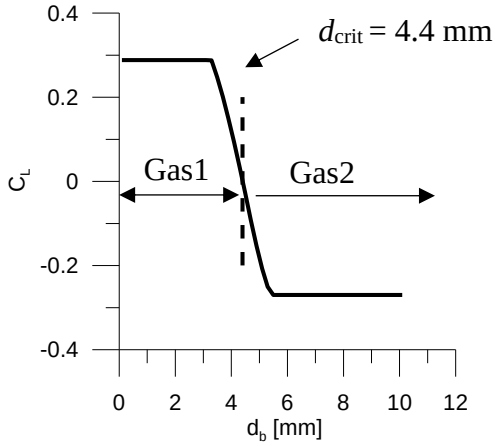

Fig. 2 Lift force coefficient for saturated steam-water systems at 20 bar according to Tomiyama et al. (2002)

The transport equation for the size fraction $f_i=\alpha_i/\alpha_g$ of group i reads

$$\frac{\partial}{\partial t}\left(\alpha_g \rho_g f_i\right) + \nabla \cdot \left(\alpha_g \rho_g f_i \vec{U}_g\right) = S_{ph,i} + S_{coal,i} + S_{br,i} + S_{nu,i}\,. \tag{15}$$

The terms on the right hand side of the equation represent sources due to phase change, coalescence, breakup and nucleation, respectively. As shown in Fig. 1, in case of boiling flows bubbles generated by nucleation on walls or in bulk are assigned to the first group. Since the representative size of bubbles in the first group is usually larger than the departure diameter at nucleation, the source term provided by the nucleation model is modified so that the interfacial area density is conserved during the assignation. The Sauter bubble mean diameter d_b of each velocity group is then calculated from the size fractions according to its definition. The present work is focused on the phase change source term $S_{ph,\,i}$. For more details about coalescence and breakup, wall and bulk nucleation the reader is referred to Liao et al. (2015) and Janet et al. (2015).

2.3 Turbulence modelling

Since eddies play an essential role in the interfacial exchanging processes, it is a key step to model the two-phase turbulence appropriately. In the present work, the turbulence behavior in the liquid phase is treated using the *k-ω* SST model, and modulation due to the presence of bubbles is considered through additional source / sink terms (Liao et al., 2011; 2018a).

$$\frac{\partial}{\partial t}\left(\alpha_{\mathrm{l}}\rho_{\mathrm{l}}k\right)+\nabla\cdot\left(\alpha_{\mathrm{l}}\rho_{\mathrm{l}}\vec{U}_{\mathrm{l}}k\right)=\nabla\cdot\left[\alpha_{\mathrm{l}}\left(\mu_{\mathrm{l}}+\frac{\mu_{\mathrm{t,l}}}{\sigma_{\mathrm{k3}}}\right)\nabla k\right]+\alpha_{\mathrm{l}}P_{\mathrm{k}}-C_{\mu}\alpha_{\mathrm{l}}\rho_{\mathrm{l}}k\omega+S_{\mathrm{k}}\ , \tag{16}$$

$$\begin{aligned}&\frac{\partial}{\partial t}\left(\alpha_{\mathrm{l}}\rho_{\mathrm{l}}\omega\right)+\nabla\cdot\left(\alpha_{\mathrm{l}}\rho_{\mathrm{l}}\vec{U}_{\mathrm{l}}\omega\right)=\\&\nabla\cdot\left[\alpha_{\mathrm{l}}\left(\mu_{\mathrm{l}}+\frac{\mu_{\mathrm{t,l}}}{\sigma_{\omega 3}}\right)\nabla\omega\right]+\left(1-F_{1}\right)2\alpha_{\mathrm{l}}\rho_{\mathrm{l}}\frac{\nabla k\nabla\omega}{\sigma_{\omega 2}\omega}+\alpha_{3}\alpha_{\mathrm{l}}\frac{\omega}{k}P_{\mathrm{k}}-\beta_{3}\alpha_{\mathrm{l}}\rho_{\mathrm{l}}\omega^{2}+S_{\omega}\end{aligned}\ . \tag{17}$$

The bubble-induced turbulence (BIT) production and dissipation is determined according to the model recently proposed by Ma et al. (2017). Its derivation was done based on an analysis of the turbulent kinetic energy budget obtained from direct numerical simulation data, and has been shown to be superior to other models purely based on dimensional analyses. The importance of taking account of the BIT as well as the effect of BIT models is presented in Liao et al. (2019).

$$S_{\mathrm{k}}=\min\left(0.18\,\mathrm{Re}_{\mathrm{p}}{}^{0.23},\,1\right)\frac{3}{4}\rho_{\mathrm{l}}\frac{C_{\mathrm{D}}}{d_{\mathrm{b}}}\left|\vec{U}_{\mathrm{g}}-\vec{U}_{\mathrm{l}}\right|^{3}, \tag{18}$$

$$S_{\varepsilon}=0.3C_{\mathrm{D}}\frac{S_{\mathrm{k}}}{d_{\mathrm{b}}}\left|\vec{U}_{\mathrm{g}}-\vec{U}_{\mathrm{l}}\right|. \tag{19}$$

And the source term for the turbulence eddy frequency S_{ω} is obtained using the transformation $\varepsilon = C_{\mu}\,\omega k$, i.e.

$$S_{\omega}=\frac{1}{C_{\mu}k}S_{\varepsilon}-\frac{\omega}{k}S_{\mathrm{k}}. \tag{20}$$

For the SST model constants σ_{k3}, $\sigma_{\omega 2}$, $\sigma_{\omega 3}$, C_{μ}, α_3, β_3 the standard values for single phase flow are used.

3. A MECHANISTIC MODEL FOR INTERPHASE HEAT TRANSFER COEFFICIENT

As shown above a correct prediction of the local heat transfer coefficient at the interface is the key in the numerical modelling of bubbly flow with thermal phase change. Due to insufficient knowledge on the dynamic mechanism governing the interphase interactions a variety of empirical correlations have been adopted in such kind of simulations. Some of them are listed in the Table 1, where the dimensionless numbers *Nu*, Re_{p}, Pr_{l}, *Ja*, *Pe* are Nusselt number, particle Reynolds number, liquid Prandtl number, Jakob number and Péclet number, respectively. Their definitions are provided in the following text.

Table 1. Examples of empirical correlations for interphase heat transfer coefficient

Correlations	**References**	**Simulated experiments**
Ranz and Marshall (1952) $Nu = 2 + 0.6Re_{\mathrm{p}}^{1/2}Pr_{\mathrm{l}}^{1/3}$ $(0 \le Re_p \le 200)$	- Chen et al. (2009) - Krepper et al. (2013) - Zhang et al. (2015) - Yang et al. (2015)	- Subcooled wall boiling

	- Murallidharan et al. (2016)	
	- Krepper et al. (2011)	- Steam condensation
	- Giese and Laurien (2002) - Liao et al. (2013)	- Flash evaporation of water
Hughmark (1967) $Nu = \begin{cases} 2 + 0.6Re_{\mathrm{p}}^{\frac{1}{2}}Pr_{\mathrm{l}}^{\frac{1}{3}} \\ \left(0 \le Re_p \le 776.06\right) \\ 2 + 0.27Re_{\mathrm{p}}^{0.62}Pr_{\mathrm{l}}^{\frac{1}{3}} \\ \left(776.06 \le Re_{\mathrm{p}}\right) \end{cases}$	- Shah et al. (2010) - Heinze et al. (2014) - Krepper et al. (2011)	- Steam condensation
Labuntzov et al. (1964) $Nu = 2 + \left(\frac{6Ja}{\pi}\right)^{1/3} + \frac{12}{\pi}Ja$	- Marsh and Withers (2006) - Maksic and Mewes (2002)	- Steam jet condensation - Flash evaporation of water
Aleksandrov (1968) $Nu = \left(\frac{12^2}{\pi^2}Ja^2 + \frac{4}{\pi}Pe\right)^{1/2}$	- Janet et al. (2015) - Liao and Lucas (2015)	- Flash evaporation of water
Tomiyama (2009) $Nu = 2 + 0.15Re_{\mathrm{p}}^{0.8}Pr_{\mathrm{l}}^{1/2}$	- Krepper et al. (2011)	- Steam condensation

Although the validity range is limited to small particle Reynolds numbers, the Ranz and Marshall (1952) correlation was used frequently for high Re_{p} cases, e.g. by Chen et al. (2009), Krepper et al. (2013), Zhang et al. (2015), Yang et al. (2015) and Murallidharan et al. (2016) for simulation of subcooled nucleate boiling. The Hughmark (1967) correlation was used by Shah et al. (2010) and Heinze et al. (2014) for steam jets condensation in subcooled water, while Marsh and Withers (2006) employed the Labuntzov et al. (1964) correlation for similar situations. In the CFD simulation of flashing flow in pipes and nozzles Giese and Laurien (2002) adopted the Ranz and Marshall (1952) correlation, while Maksic and Mewes (2002), Janet et al. (2015), Liao and Lucas (2015) used the ones presented in Labuntzov et al. (1964) and Aleksandrov (1968), respectively. On the other hand, Krepper et al. (2011) and Liao et al. (2014) showed that the applied correlations have a significant influence on the prediction of steam void fraction in a condensing steam-water flow. The Ranz and Marshall (1952) and Hughmark (1967) correlations were found to under-predict the condensation rate, while the Tomiyama (2009) correlation give an obvious over-prediction. A detailed evaluation on these correlations under flashing conditions was conducted by Liao and Lucas (2017; 2018b).

The arbitrariness and uncertainty encountered in choosing the empirical correlations indicates that development of a mechanistic model based on sound understanding of local phenomena is of essential importance for reliable simulations. As shown in Fig. 3 the interphase heat transfer process is governed by the superposition of three mechanisms, i.e. (a) conduction due to temperature gradient; (b) convection due to relative motion; (c) surface renewal due to turbulence eddies. The conduction and convection are two fundamental modes of heat transfer

caused by physical contact and relative motion of the two objects between which the heat transfer takes place. The surface renewal mechanism refers to the scenario that under turbulent conditions eddies from the bulk regularly bombard the bubble surface, and bring heat to or take heat away from the bubble depending on the liquid is superheated or subcooled. It envisions that the contact surface between the liquid and the bubble is constantly renewed by the turbulence eddies, which bring fresh liquid elements from the bulk to the interface and replace the "old" ones, see Fig. 3(c). The contribution of each of the mechanisms in a heat transfer process depends on temperature, velocity difference as well as turbulence intensity.

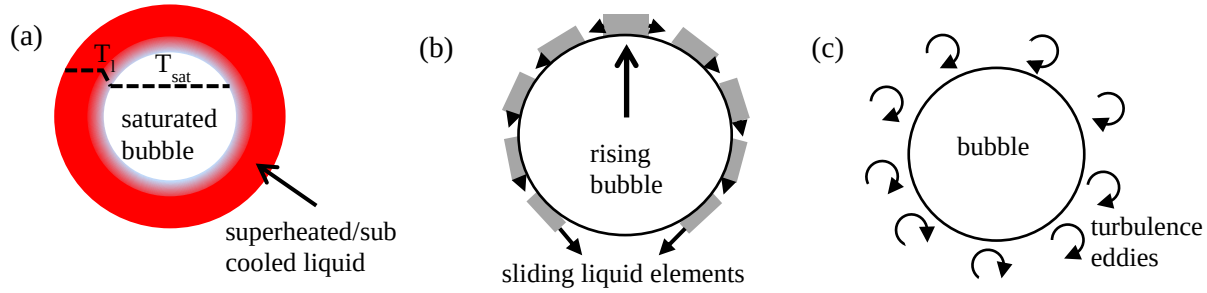

Fig. 3 Interphase heat transfer mechanisms: a) conduction b) convection (Morsi and Basha, 2015) c) surface renewal

Mechanistic models are available for each individual mechanism under ideal conditions. For example, by assuming a constant liquid bulk temperature and a stationary "thin thermal boundary layer" (see Fig. 3a) the Nusselt number of conduction heat transfer may be expressed as

$$Nu_{\mathrm{cond}} = K_{\mathrm{s}}^{\,2}\,\frac{4}{\pi}\,Ja\,, \tag{21}$$

where K_{s} is a so-called spherical correction factor (Birkhoff et al., 1958). For semi-infinite plane slab K_{s}=1.0, while for spherical bubbles a value larger than 1 is used, e.g. in Plesset and Zwick (1954) $K_{\mathrm{s}} = \sqrt{3}$ while in Forster and Zuber (1954) $K_{\mathrm{s}} = \pi/2$. The Jakob number Ja is defined as

$$Ja = \frac{\rho_{\mathrm{l}} c_{\mathrm{p,l}} \left| T_{\mathrm{sat}} - T_{\mathrm{l}} \right|}{\rho_{\mathrm{g}} L}\,, \tag{22}$$

wherein L represents the latent heat for phase change. The "thermal boundary layer" conceptualization is popular because of its simplicity. However, it should be noted that the validity of the "thin thermal boundary layer" assumption is limited to highly simplified situations, e.g. (i) quiescent and stationary state; (ii) isothermal and uniformly superheated liquid of infinite extent; (iii) constant pressure field. In practical cases, these conditions hardly can be satisfied and convection is always present in the liquid due to the translational motion of bubbles. Ruckenstein and Davis (1971) showed that at low and moderate Jakob numbers, the contribution of convection can be significant if the translation motion is sufficiently high. For convective heat transfer coefficient, the "penetration theory" or the Higbie model (Higbie, 1935) is widely used. The basic assumptions behind the theory are: (1) all liquid elements come into contact with the bubble at the bubble nose, sliding along the bubble surface and detaching at the rear of the bubble; (2) heat transfer between the bubble and a liquid element occurs as long as they are in contact; (3) each of the liquid elements stays in contact with the bubble for

the same duration (see Fig. 3b). The heat transfer coefficient can be expressed in terms of the contact time, which is determined by

$$\tau_{\mathrm{conv}} = \frac{d_{\mathrm{b}}}{\left|\vec{U}_{\mathrm{g}} - \vec{U}_{\mathrm{l}}\right|}\,. \tag{23}$$

For potential flow, the quasi steady state approximation of the Nusselt number is given by (Ruckenstein and Davis, 1971)

$$Nu_{\mathrm{conv}} = \frac{2d_{\mathrm{b}}}{\sqrt{\pi a_{\mathrm{l}} t_{\mathrm{conv}}}} = \frac{2}{\sqrt{\pi}} Pe^{1/2}\,, \tag{24}$$

where the Péclet number *Pe* is defined as

$$Pe = \frac{d_{\mathrm{b}}\left|\vec{U}_{\mathrm{g}} - \vec{U}_{\mathrm{l}}\right|}{a_{\mathrm{l}}} = \mathrm{Re}_{\mathrm{p}} \cdot \mathrm{Pr}_{\mathrm{l}}\,. \tag{25}$$

According to Ruckenstein and Davis (1971) when the Jakob number is of the order of square Péclet number both conduction and convection terms are significant in determining the heat transfer coefficient.

The assumption of uniform residence time of the liquid elements on the bubble surface is apparently too simple. Above “penetration theory” based on the potential flow theory fails in elucidating random and chaotic migration of small fluid elements (eddies) from the bulk to the interface under turbulent conditions. It is commonly known that the transfer rate is enhanced by the turbulence. The “surface renewal theory” is frequently used for the interpretation of the turbulence intensification, which aims to describe the interfacial transfer more close to the realistic picture by incorporating some statistical components, e.g. in the distribution of the contact time. The “surface renewal theory” is a kind of modification of the “penetration theory”, and the expression for Nusselt number in Eq. (24) is further usable just by replacing the time scale t_{conv} by an appropriate time scale for eddies. According to the statistical expression used for the contact time distribution, numerous variants of the “surface renewal theory” have been proposed (Fan et al., 1993). Danckwerts (1951) suggested that the contact times of eddies are completely random or exponentially distributed, while for the purpose of generality Perlmutter (1961) proposed an expression for the contact time by blending the completely random distribution with the uniform distribution. Although the surface renewal theory is physically more advantageous in the description of interphase transport processes than the stagnant film or penetration theory, it is less popular in the two-fluid modelling of bubbly flows. One reason is supposed to be that the statistical or stochastic expressions proposed for the contact time between the eddy and the bubble are mostly less compatible with the continuum models and deterministic mathematics. In the domain of stratified gas-liquid flows the interphase heat transfer correlations based on surface renewal theory, which are used to predict the heat transfer coefficient at the large gas-liquid interface, are often expressed in terms of the characteristic time scale of eddies (Fortescue and Pearson, 1967; Banerjee et al., 1968; Lakehal and Labois, 2011).

$$\tau_{\mathrm{turb}} = \frac{l_{\mathrm{turb}}}{u_{\mathrm{turb}}}\,. \tag{26}$$

In the RANS context, the characteristic length and velocity scales of energy-containing eddies are determined by the turbulent kinetic energy k and its rate of dissipation ε

$$l_{\mathrm{turb}} = C_{\mu}^{3/4} \frac{k^{3/2}}{\varepsilon}, \quad u_{\mathrm{turb}} = C_{\mu}^{1/4} k^{1/2}.$$

The model based on these scales is referred to as a large eddy model (Fortescue and Pearson, 1967). Alternatively, small eddy models, which are based on the scales of eddies in the viscous subrange (Banerjee et al., 1968), and hybrid models blending the two subranges are available for the determination of the time scale (Ceuca, 2015). The Nusselt number considering eddy contribution is derived by substituting Eq. (26) into Eq. (24)

$$Nu_{\mathrm{turb}} = \frac{2}{\sqrt{\pi}} \mathrm{P}e_{\mathrm{t}}^{1/2} \frac{d_{\mathrm{b}}}{l_{\mathrm{turb}}}. \tag{27}$$

And the turbulent Péclet is defined by

$$Pe_{\mathrm{t}} = \mathrm{Re}_{\mathrm{t}} \cdot \mathrm{Pr}_{\mathrm{l}}, \tag{28}$$

where Re_{t} represents the turbulent Reynolds number, expressed as

$$\mathrm{Re}_{\mathrm{t}} = \frac{l_{\mathrm{turb}} u_{\mathrm{turb}}}{\nu_{\mathrm{l}}}. \tag{29}$$

If the gas-liquid interface in a stratified flow is considered as a large bubble moving in the liquid, the model can be used in analogy to simulate the interphase heat transfer induced by turbulence in bubbly flows. Combining with heat conduction, translational convection the three heat transfer mechanisms play a joint role in a turbulent bubbly flow, and the individual contribution depends on the magnitude of temperature difference, relative velocity as well as turbulence intensity at the interface. Without further knowledge their effects are assumed cumulative as done in many previous works. Whitaker (1972) interpreted that the enhancement in transfer rates between a sphere and the surrounding liquid due to the presence of turbulence comes purely from the wake contribution, and it is cumulative to the laminar part. Wolfert et al. (1978) combine the three terms resulting from conduction, convection and turbulence linearly

$$Nu = \left(\frac{12}{\pi} Ja + \frac{2}{\sqrt{\pi}} Pe^{1/2} + \frac{2}{\sqrt{\pi}} Pe^{1/2} \frac{\lambda_{\mathrm{t}}}{\lambda_{\mathrm{l}}} \right), \tag{30}$$

and introduce a so-called eddy conductivity λ_{t}, which is adjusted to 0.8. It envisions that the liquid boundary surrounding the bubble surface consists of dissimilar material and the heat transfer resistances are in parallel. The same approach replacing the last term with Eq. (27) is adopted in the present work, and the overall Nusselt number is then given by

$$Nu = \left(\frac{12}{\pi} Ja + \frac{2}{\sqrt{\pi}} Pe^{1/2} + \frac{2}{\sqrt{\pi}} Pe_{\mathrm{t}}^{1/2} \frac{d_{\mathrm{b}}}{l_{\mathrm{turb}}} \right). \tag{31}$$

Note that in case of more than one velocity groups the interfacial heat transfer is calculated for each velocity group j, and d_{bj} is the corresponding Sauter mean diameter for the velocity group j. The heat and mass flux is apportioned to the size groups inside the velocity group according to their fractions f_i (Liao et al., 2014).

4. MODEL VALIDATION

The new model is validated at first for the case of bubble growth in superheated water under different conditions, where either conduction or convection or turbulence plays a dominant role in controlling the interphase heat transfer rate. In this way the components in the model for these effects can be tested separately to a certain extent. As follows, it is used for the simulation of steam bubbles condensing in flowing sub-cooled water through a vertical pipe, for which CFD-grade data of phase distribution and bubble size are available.

4.1 Bubble growth in superheated liquid

For the validation of the conduction, convection and turbulence components in the model the following three cases are considered, which all concern with steam bubbles growing in superheated water.

- Case 1: bubble growth in stagnant uniform superheated liquid under zero-gravity condition;
- Case 2: bubble growth in stagnant uniform superheated liquid under normal-gravity condition;
- Case 3: bubble growth in turbulent superheated liquid flow.

The first two test cases are taken from the experiments of Florschuetz et al. (1969), in which the water is stagnant and has uniform and constant initial superheats. The growth of microscopic bubbles that present naturally in the liquid volume are realized by suddenly reducing the system pressure. The zero gravity condition in Case 1 is achieved by releasing the experimental vessel with the camera from the mount frame and dropping it to a sand box. The data on bubble growth in flowing superheated water are provided by Avdeev (2016), while the experiments were conducted by Kol'chugin et al. (1976) and Lutovinov (1985). These experiments are characterized by a high turbulence level, and the bulk water flow velocity U_b ranges from 16 to 24 m/s. The relevant parameters describing the experimental conditions of the three cases are given in Table 2.

Table 2 Experimental conditions of the investigated cases

Cases	**p [MPa]**	**T_{sup} [K]**	**g [m s^{-2}]**	**U_b [m s^{-1}]**	**Ja**	**Pe**	**Pe_t**	**References**
1	0.1	2.9	0.0	0	8.69	0	0	Florschuetz et al. (1969)
2	0.1	3.9	9.8	0	10.98	10^4	0	Florschuetz et al. (1969)
3	2.0	1.0	9.8	16~24	0.19	22	27	Avdeev (2016)

The comparison between the measured and calculated transient bubble radius as well as the prediction using the Ranz and Marshall (1952) correlation is shown in Fig. 4.

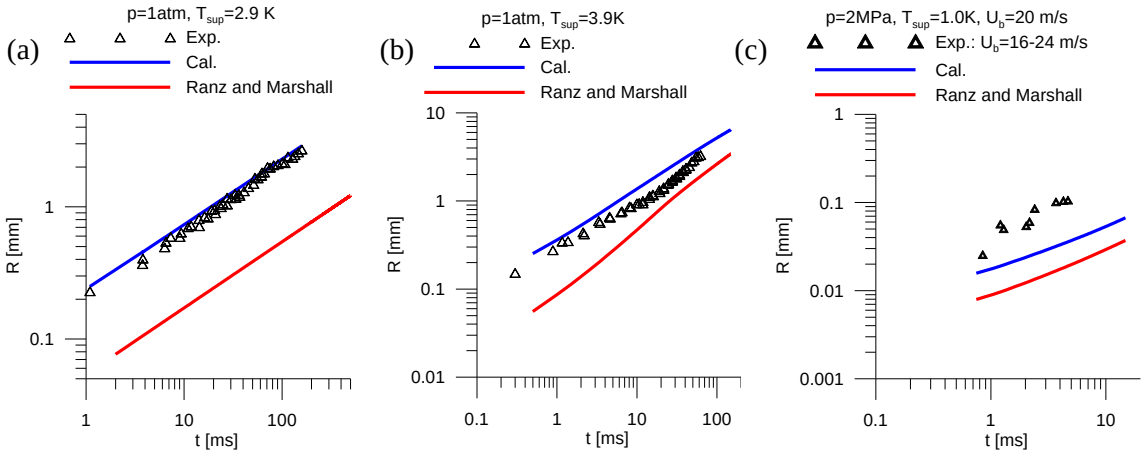

Fig. 4 Prediction of bubble growth in superheated liquid: (a) Case 1 (b) Case 2 (c) Case 3

In Case 1 conduction alone plays a role in controlling the interfacial heat transfer process, and the contribution of other two components is zero. Excellent agreement between the measurement and calculation is achieved, while the widely-used Ranz and Marshall (1952) correlation under-predicts the bubble growth rate significantly. That means that the asymptotic value of 2 in the correlation (see Table 1) is insufficient to describe the heat conduction rate in this case, which is also confirmed by Walton (2004) in his experimental study on the evaporation of water droplets in hot air.

In Case 2 due to the gravitational effect, bubbles are translating during their rising. The translational motion enhances the overall heat transfer and thus bubble growth rate considerably. The effect of convection due to the translation increases as the bubble grows. Obvious under-prediction by the Ranz and Marshall (1952) correlation is present at the beginning, while disappears at the later growth stage as expected, when the effect of heat conduction becomes negligible.

For the case of flowing liquid there are extremely limited data available, and as a consequence appropriate models are scarce. Relations obtained for the bulk of still liquid are frequently applied in the numerical and theoretical study on bubble growth in flowing superheated liquid. However, the validity of this extrapolation is not ensured as pointed out by Avdeev (2016), who shows that none of the relations are suitable for the description of bubble growth in a flow of superheated liquid obtained by Kol'chugin et al. (1976) and Lutovinov (1985). For the cases with p=2 MPa, T_{sup}=1 K and U_b=16-24 m/s, the transient bubble radius is shown in Fig. 4 (c). It evidences that the prediction by the mechanistic model presented in this work is more close to the measurement than that by the Ranz and Marshall (1952) correlation, although they both under-predict the growth rate. Unfortunately, there is no information about the experimental uncertainty, but the photography shows that the shape of bubbles is always irregular and highly instable due to the strong dynamical turbulent effect.

4.2 Bubble condensing in subcooled liquid

The model incorporating the three mechanisms of conduction, convection and turbulence is used for the simulation of condensing steam-water pipe flow, which may be encountered in many nuclear engineering applications. For comparison the K16 experiments carried out in the TOPFLOW facility at the Helmholtz-Zentrum Dresden - Rossendorf are used. Subcooled water flows upward through a vertical DN200 pipe and saturated steam is injected from the circumferential surface at the lower part of the pipe via orifices (see Fig. 5a). The volume

fraction of steam decreases along the pipe due to condensation, and the development of steam velocity and distribution in the pipe are obtained by using the wire-mesh sensors. Experiments were performed for several gas and liquid volumetric fluxes J_g and J_l, inlet subcooling $T_{sub,in}$, orifice opening $D_{orifice}$ and pressure levels p. High-resolution measurements of steam volume fraction, steam velocity, bubble size distribution as well as water temperature are available for different height positions. The test facility and measurement technique have been described at length elsewhere (Krepper et al., 2011; Liao et al., 2014; Liao and Lucas, 2016). The experimental conditions of the case investigated in this work are summarized in Table 3. The pressure at the steam injection position is kept at 20 bar.

Table 3 Experimental conditions of the test case

J_l [m/s]	J_g [m/s]	$T_{sub,in}$ [K]	$D_{orifice}$ [mm]	p [bar]
1.017	0.219	6.0	1.0	20

As shown in the previous work of Krepper et al. (2011) and Liao et al. (2014) reliable prediction of the interphase heat transfer rate is crucial in getting accurate condensation rates and volume fractions. The simulation is carried out using the commercial software ANSYS CFX, and each step is set appropriately and checked carefully according to the BPG regarding mesh generation, boundary condition setup as well as convergence behavior monitoring.

4.2.1 Geometry model and grid

In order to avoid the disturbance and uncertainty introduced by steam injection, the computational domain begins at 1.552 m above the injection position, see Fig. 5a), where a stable steam-water upward flow is present. Bubble coalescence is shown to have an effect within downstream a distance of one meter from the injection (Liao et al., 2014; Liao and Lucas, 2016). The distance between the injection and the inlet boundary (Level I) as well as two other measurement planes (Level L and Level O) is listed in Table 4.

Table 4 Heights relative to the steam injection position

Steam injection	Level I	Level L	Level O
0.0 [m]	1.552 [m]	2.595 [m]	4.531 [m]

In addition, for high computational efficiency a small cylindrical sector (θ=4°) instead of the whole pipe is simulated with the assumption of axisymmetric flow. The simplification is justified by both experimental and numerical observations (Krepper et al., 2011).

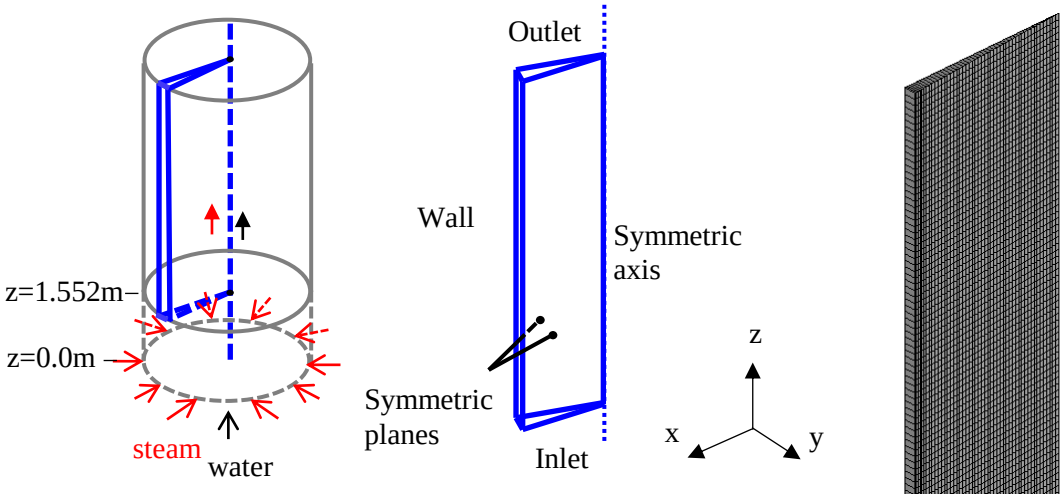

(a) (b) (c)

Fig. 5 Schematic representation of the geometry model and computational grid

As shown in Fig. 5c) a quasi two-dimensional mesh is applied to the cylindrical sector. That means that there are only one layer of cells in the azimuthal direction, and the front and back are symmetrical planes, see Fig. 5b). The geometry and grid is generated using the ICEM CFD software and the mesh quality is checked according to the recommended criteria (Ansys, 2018). The small connection angle of the two symmetric planes is shown to have no impact on the convergence behavior. To achieve mesh-independent results, mesh studies are performed in advance. As shown in Table 5, three meshes have been applied, which have total nodes of 13x313x1, 25x625x1 and 50x1250x1, respectively.

Table 5 Details of mesh statistics

Mesh	N	N_x	N_z	N_y	Δx_{min}[mm]	Δx_{max}[mm]	Δz_{min}[mm]	Δz_{max}[mm]
coarse	13x313x1	13	313	1	4.0	13.6274	4.0	16.4071
medium	25x625x1	25	625	1	2.0	4.7159	2.0	8.10584
fine	50x1250x1	50	1250	1	1.0	2.10278	1.0	4.02612

As shown in Fig. 6 the results obtained by the medium mesh can be considered as mesh independent. Slight difference is observed at the peak of radial gas volume fraction profiles, see Fig. 6 (a), while the bubble size distribution and liquid temperature profiles coincide with each other. The findings are consistent with the previous work of Liao and Lucas (2016), where the Ranz-Marshall correlation is adopted. The update of the interphase heat transfer coefficient does not change the mesh dependency noticeably. All results presented below are obtained with the fine mesh in Table 5.

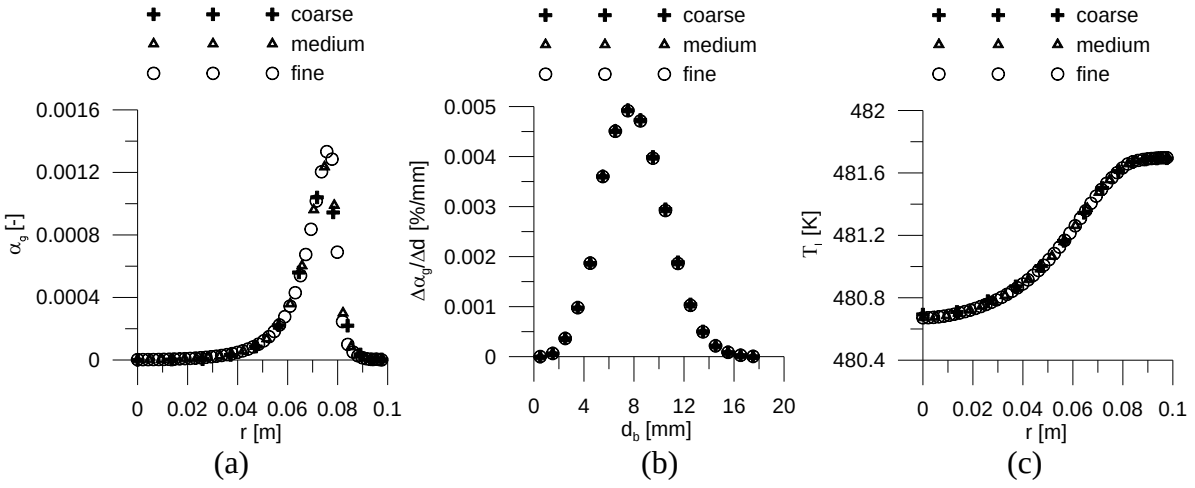

Fig. 6 Results of mesh independency study. (a) gas volume fraction (b) bubble size distribution (c) liquid temperature

4.2.2 Initial, boundary conditions and material properties

As illustrated in Fig. 5b), there are four types of boundary conditions applied in the simulation, namely, inlet, outlet, wall and symmetry. The inlet conditions for the steam phase including volume fraction, velocity and bubble size distribution are defined according to experimental data. For the liquid phase the temperature profile is provided by the measurements, but data for determining velocity and turbulence intensity are missing. Fully-developed single phase

profiles are assumed for turbulence parameters. The velocity profile is assumed to be identical to that of the gas phase, and the magnitude is calculated according to the superficial velocity given by the experimental condition. Pressure outlet boundary conditions are applied. The static pressure at the outlet boundary is prescribed constant, which is approximately equal to pressure measured at the steam injection position minus the hydrostatic pressure of the water. The solid wall is assumed adiabatic and smooth, at which the liquid has no-slip conditions while the steam has free-slip ones. The velocity of the fluid immediately next to a no-slip wall is equal to zero. A free-slip wall assumes that the shear stress at the wall in the flow direction is zero and the velocity of the fluid near the wall is not retarded by wall friction effects, while the velocity perpendicular to the flow direction is zero. The initial condition in the simulation domain is sub-cooled pure water, and the temperature, velocity and turbulence are initialized with the inlet profiles. The initial and boundary conditions applied in the simulation are shown to be stable. The steam and water properties vary with pressure and temperature locally according to the international standard IAPWS-IF97 tables. The phase boundary or vapor pressure curve between water and steam is determined by defining a homogeneous binary mixture (Ansys, 2018). The curve is used then by the solver to determine the saturation properties of the two materials.

4.2.3 Numerical schemes and convergence criteria

In the simulation the coupled volume fraction algorithm was used, which allows the implicit coupling of the velocity, pressure and volume fraction equations. The high resolution scheme was selected to calculate the advection terms in the discrete finite volume equations. The discretization algorithm for the transient term was the second order backward Euler. The upwind advection and the first order backward Euler transient scheme were used in the turbulence numerics.

The convergence of the simulations was checked with strict criteria. For example, the maximum residual for the mass, momentum and energy equations is set to 10^{-5}, while that for the turbulence and size fractions set to 10^{-4}. It is an important measure of the local imbalance of each conservative control volume equation. Small values of domain imbalance ($\leq$0.1%) indicate that the global conservation of all transport equations has essentially been achieved. The maximum equation residual of the simulation that presented in this work is shown in Fig. 7, where (a) are the mass equations, (b)-(d) the momentum equations in the x, y and z directions; (e) and (f) energy and turbulence equations, respectively, (g)-(i) the size fraction equations of MUSIG groups 1 – 15. As one can see, all the prescribed convergence criteria are satisfied by the presented simulation results after 5000 time steps when the steam-water mixture reaches the top of the pipe.

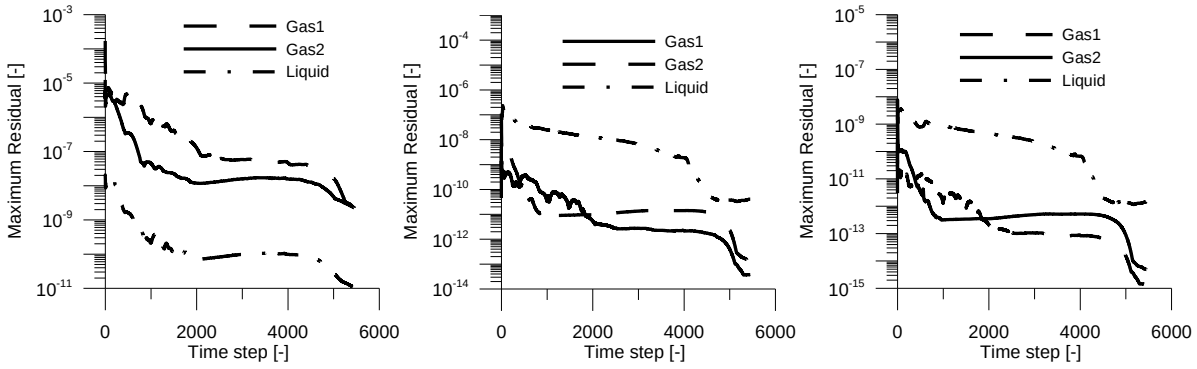

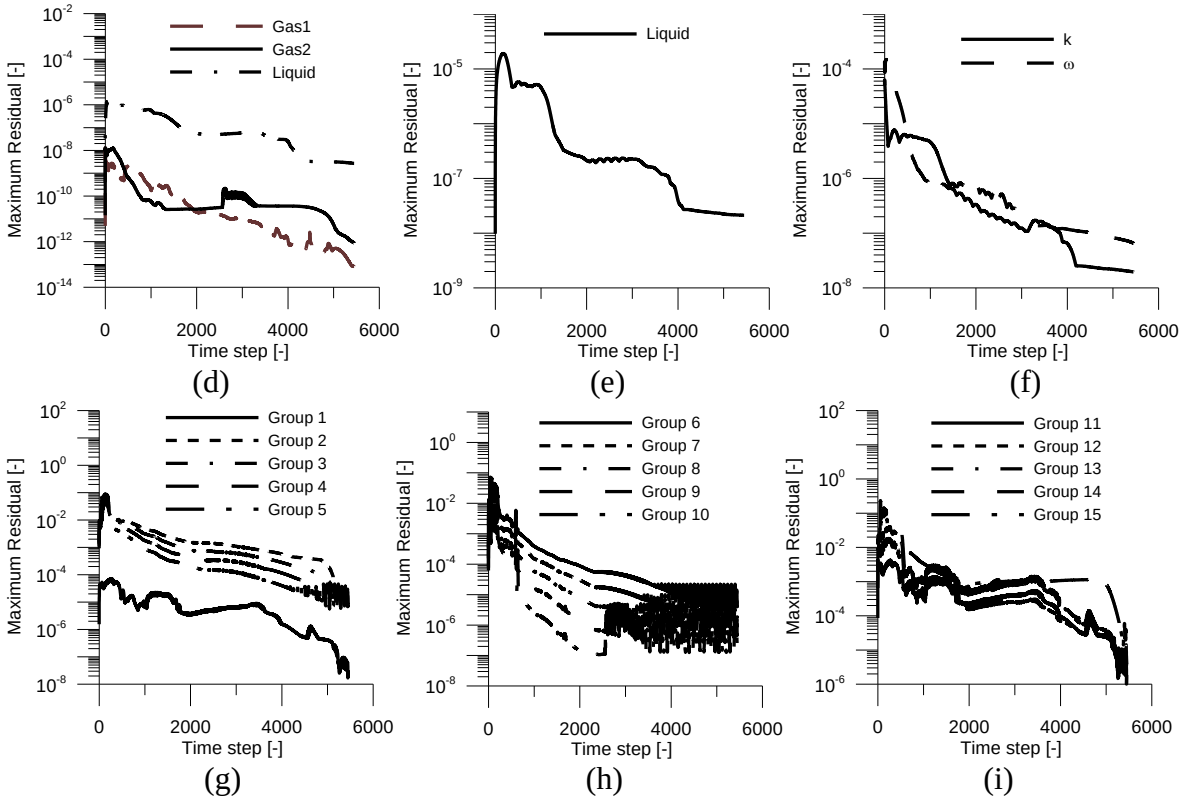

Fig. 7 Maximum residuals of the solved transport equations: a) mass equations; b) momentum equations in x direction; c) momentum equations in y direction; d) momentum equations in z direction; e) energy equation; f) k and ω equations; g) - i) MUSIG size fraction equations (Group 1 – Group 15)

4.2.4 Simulation results

The simulated and measured radial gas volume fraction profiles at the three levels (see Table 4) are shown in Fig. 8, where the crosses represent experimental data, and the dash and solid lines are predictions using the Ranz-Marshall correlation and the mechanistic model presented in this work, respectively. Because of condensation the steam volume fraction decreases as the steam-water mixture flows from Level I to Level O. The decreasing rate evidences that the Ranz-Marshall correlation under-predicts the condensation rate significantly, while the new model achieves a quantitatively good agreement with the measurement. In this case it is found that the heat conduction Nusselt number is two orders of magnitude lower than the convection and turbulence ones. The turbulence enhancement is strong especially in the near-wall region where the turbulence level is high. The Ranz-Marshall correlation fails to reproduce the effect, but the mechanistic model succeeds. Furthermore, the radial distribution of steam at all the three levels possesses a wall-peak profile because the steam is injected into the bulk liquid from the pipe wall. The peak shifts slightly to the center of the pipe as a result of the lateral lift force, since the Sauter mean bubble diameter is larger than the critical value provided by Tomiyama et al. (2002), see Fig. 2.

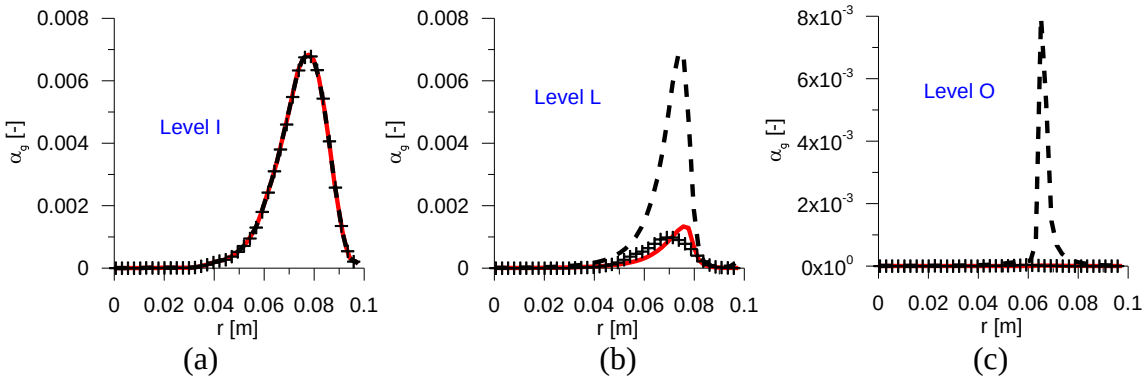

Fig. 8 Radial profile of gas volume fraction at Level I, L and O (cross: experiment, dash line: Ranz-Marshall correlation, solid line: new model)

The cross-section averaged bubble size distribution at the three levels is shown in Fig. 9, which is defined as the volume fraction of each MUSIG size group divided by the bin width, i.e. $\Delta\alpha_g/\Delta d$. One can see that the maximum value of the distribution decreases as a result of condensation. In addition, from Level I to Level O the distribution becomes narrower and the peak moves towards small bubble diameter due to bubble shrinkage. These effects are all captured by the numerical model as the mixture flows from Level I to Level L. In contrast, the Ranz-Marshall correlation under-estimates the shrinkage rate seriously due to a too small condensation rate.

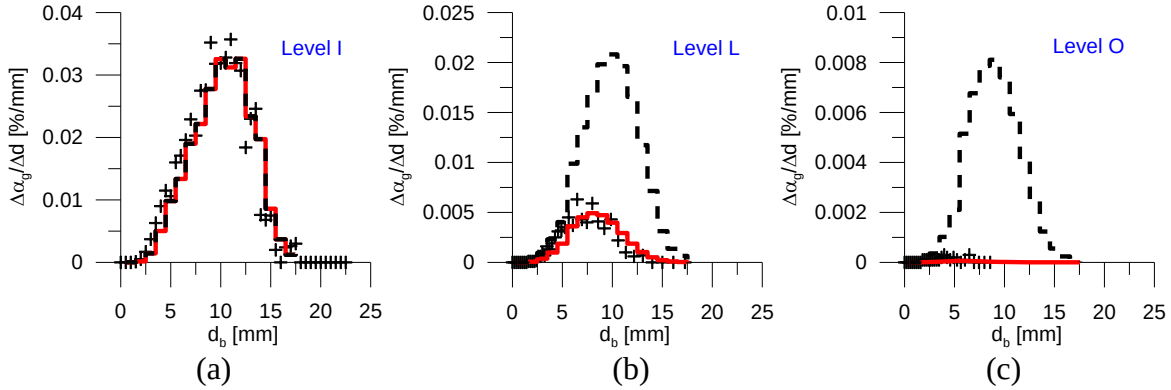

Fig. 9 Cross-section averaged bubble size distribution at Level I, L and O (cross: experiment, dash line: Ranz-Marshall correlation, solid line: new model)

The comparison of radial liquid temperature profile is illustrated in Fig. 10. As mentioned at the beginning, the liquid temperature in the domain is initially uniform before the injection of the steam. Due to the heat released by steam condensation the liquid is warmed up. And corresponding to the wall-peak profile of steam volume fraction, the liquid temperature near the wall becomes higher than that in the center of the pipe. At the upper part of the pipe steam volume fraction and condensation rate is sufficiently low, and the radial temperature gradient disappears gradually as a result of diffusion and convection. The diffusion effect in the radial direction is however not well captured by the model. It indicates that further investigation regarding two-phase turbulence or turbulent diffusion modelling is necessary. This is a topic for future research. In the present work, the turbulent heat flux is modelled by the eddy diffusivity hypothesis (see Eq. 3), and the turbulent Prandtl number Pr_t is set to 0.9. Nevertheless, the absolute deviation is less than 0.5 K, see Fig. 10(c). Additionally, the

predictions using the Ranz-Marshall correlation and the model presented in this work are nearly identical at all levels. This is because the total steam volume fraction in the pipe section from Level I to Level O is pretty low (<1%), and the heat released by steam condensation is too little to increase the liquid temperature considerably.

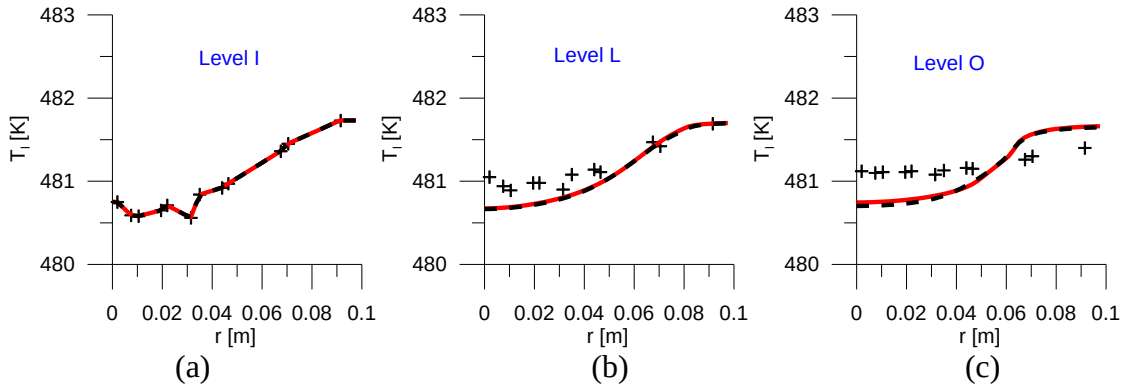

Fig. 10 Radial profile of liquid temperature at Level I, L and O (cross: experiment, dash line: Ranz-Marshall correlation, solid line: new model)

The evolution of average gas volume fraction, Sauter mean bubble diameter and liquid temperature along the flow direction (pipe axis z) is demonstrated in Fig. 11. In contrast to the empirical correlation of Ranz and Marshall (1952) the mechanistic model reproduces the experimental data reliably. Slight deviation regarding gas volume fraction and bubble diameter is present at the top of pipe, where the total steam volume fraction is negligibly low ($\alpha_g \leq 10^{-5}$), and in this case the measurement error increases dramatically. The good agreement achieved in all three parameters evidences the reliability of the suggested model. It is worth mentioning that all the results are achieved under the guideline of baseline closure concept and there are no empirical constants and adjustments necessary.

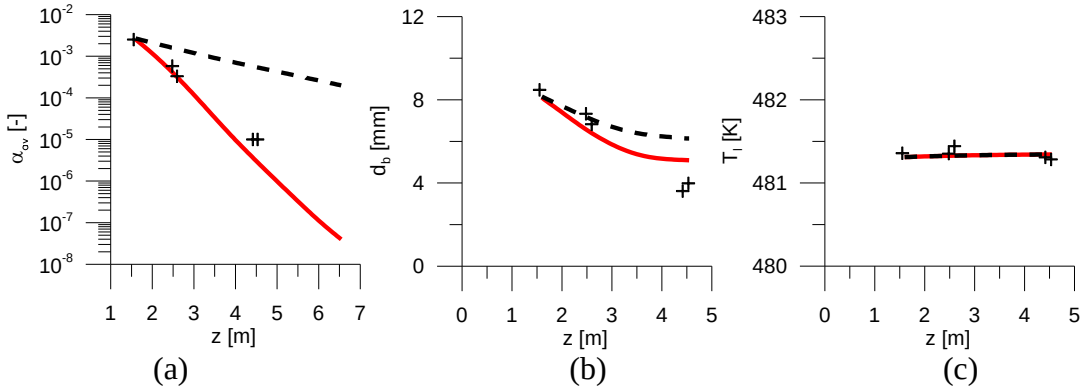

Fig. 11 Cross-section averaged a) gas volume fraction, b) Sauter mean diameter, c) liquid temperature (cross: experiment, dash line: Ranz-Marshall correlation, solid line: new model)

5. CONCLUSION

Computational fluid dynamics is becoming an important tool in nuclear safety analysis, but it should be cautioned that applying predictive models is the prerequisite and extrapolation of empirical correlations is dangerous. The predictability of a model is ensured only when the local flow phenomena or mechanisms are represented correctly. Due to its high complexity sound knowledge on interphase transfer phenomena in multiphase flows so far is insufficient.

There is still a long way to go before predictive multiphase models are available although large progress has been made in the past several decades in the computational fluid dynamics. Currently, most simulations are limited to post-test or reproduce the experimental data with a certain combination of closures. The applied models are far from the predictability, and as a result the case-by-case tuning is inevitable. The baseline closure concept initiated by HZDR is aimed at improving the predictability of models for two-fluid modelling of multiphase flows. To avoid the fact that the imperfectness of a model is covered by different combination of models or artificial tuning, the concept prescribes a fixed set of models and model constants. The concept is shown to be helpful in finding out model insufficiency and aspects that need further development. In the present work, a mechanistic model free of empiricism is proposed for the calculation of interfacial heat transfer coefficient using the baseline closure concept. It is tested in well-defined simulations for condensation and evaporation by employing the BPG. From the comparison with the experimental data following conclusions can be drawn:

1) The mechanistic model taking account of heat conduction, convection and turbulence is effective in predicting the interphase heat transfer coefficient in bubbly flow.
2) A general improvement is evidenced by the presented model in cases ranging from stationary bubble growth to bubble condensing in turbulent flow in comparison with the widely-used Ranz-Marshall correlation (Ranz and Marshall, 1952).
3) Data for validating the contribution of various heat transfer mechanisms separately are insufficient especially regarding the turbulence effect. Future efforts should be made in acquiring more reliable data by means of experiment or DNS simulation.

NOMENCLATURE

a_l	Liquid thermal diffusivity	$m^2 \cdot s^{-1}$	Nu_{turb}	Nusselt number for heat transfer due to turbulence eddies	
A_{lg}	Interfacial area density	m^{-1}	Nu_{conv}	Nusselt number for convective heat transfer	
$c_{p,l}$	Isobaric specific heat capacity	$J \cdot kg^{-1} \cdot K^{-1}$	p	Pressure	Pa
C_μ	Standard eddy viscosity model constant		P_k	Production term of turbulent kinetic energy	$kg \cdot m^{-1} \cdot s^{-3}$
C_D	Drag coefficient		Pe	Péclet number	
C_L	Lift force coefficient		Pe_t	Turbulent Péclet number	
d_b	Sauter mean bubble diameter	m	Pr_l	Prandtl number	
d_{crit}	Critical bubble diameter for lift force changing the sign	m	Pr_t	Turbulent Prandtl number	
$D_{orifice}$	Diameter of gas injection orifice	m	q_{lg}	Heat flux into the liquid phase flow the interface	$W \cdot m^{-3}$
F_1	First blending function of k-ω SST model		Re_p	Particle Reynolds number	
$\vec{F}_{lg}$	Volumetric interfacial force acting on liquid phase by gas phase	$kg \cdot m^{-2} \cdot s^{-2}$	Re_t	Turbulent Reynolds number	
f_i	Volume fraction ratio of size group i, also called size fraction, defined by $\alpha_{g,i}/\ \alpha_g$		S_k	Bubble-induced source terms for k	$m^2 \cdot s^{-3}$

$\vec{g}$	Gravitational acceleration	$m \cdot s^{-2}$	S_ω	Bubble-induced source terms for ω	s^{-2}
h_l	Overall heat transfer coefficient between liquid phase and the interface	$W \cdot m^{-2} \cdot K^{-1}$	S_ε	Bubble-induced source terms for ε	$m^2 \cdot s^{-4}$
H_l	Liquid static enthalpy	$J \cdot kg^{-1}$	$S_{br,i}$	Source/sink term of size group i due to bubble breakup	$kg \cdot m^{-3} \cdot s^{-1}$
$H_{tot,g}$, $H_{tot,l}$	Total enthalpy of gas and liquid phase	$J \cdot kg^{-1}$	$S_{coal,i}$	Source/sink term of size group i due to bubble coalescence	$kg \cdot m^{-3} \cdot s^{-1}$
$H_{tot,gi}$, $H_{tot,li}$	Total enthalpy of gas and liquid phase at the interface	$J \cdot kg^{-1}$	$S_{nu,i}$	Source term of size group i due to bubble nucleation	$kg \cdot m^{-3} \cdot s^{-1}$
$H_{tot,gs}$, $H_{tot,ls}$	Total enthalpy of gas and liquid phase at the saturation condition	$J \cdot kg^{-1}$	$S_{ph,i}$	Source/sink term of size group i due to phase change	$kg \cdot m^{-3} \cdot s^{-1}$
i	Index of the bubble size fraction group		$S_{E,lg}$	Source/sink term of liquid energy equation due to phase change	$W \cdot m^{-3}$
J	Index of the bubble velocity group		$S_{M,lg}$	Source/sink term of liquid /gas momentum equation due to phase change	$kg \cdot m^{-2} \cdot s^{-2}$
Ja	Jakob number		S_{lg}	Source/sink term of liquid /gas mass equation due to phase change	$kg \cdot m^{-3} \cdot s^{-1}$
J_g, J_l	Superficial gas and liquid velocity	$m \cdot s^{-1}$	T_l	Liquid temperature	K
K_s	Form correction factor for heat conduction across the interface		$T_{sub,in}$	Liquid inlet sub-cooling	K
k	Turbulent kinetic energy	$m^2 \cdot s^{-2}$	T_{sup}	Liquid superheating	K
L	Latent heat	$J \cdot kg^{-1}$	T_{sat}	Saturation temperature	K
l_{turb}	Turbulence length scale		$\vec{U}_g$	Gas velocity vector	$m \cdot s^{-1}$
M_J	Total number of bubble size groups in the velocity group J		$\vec{U}_l$	Liquid velocity vector	$m \cdot s^{-1}$
N	Total number of velocity groups		$\vec{U}_{g,1}$, $\vec{U}_{g,2}$	Velocity vector of the velocity group 1, 2, respectively	$m \cdot s^{-1}$
Nu_{cond}	Nusselt number for heat conduction		u_{turb}	Turbulent velocity scale	$m \cdot s^{-1}$
			U_b	Liquid bulk velocity	$m \cdot s^{-1}$

Greek letters

α_g, α_l	Liquid, gas volume fraction		μ_l, $\mu_{t,\,l}$	Liquid, liquid eddy viscosity	Pa·s
α_i	Volume fraction of size group i		ρ_l, ρ_g	Liquid, gas density	$kg \cdot m^{-3}$
α_{max}, α_{min}	Minimum and maximum gas volume fraction for calculation of interfacial area density		ω	Turbulence eddy frequency	
α_3	k-ω SST model constant		π	A mathematical constant	
β_3	k-ω SST model constant		σ_{k3}, $\sigma_{\omega 3}$, $\sigma_{\omega 2}$	k-ω SST model constant	
ε	Turbulence dissipation rate	$m^2 \cdot s^{-3}$			

Γ_{lg}	Interfacial mass transfer rate from gas to liquid	$kg \cdot m^{-3} \cdot s^{-1}$	τ_{conv}	Time scale for convective heat transfer at the interface due to relative velocity	s
Γ_{gl}	Interfacial mass transfer rate from liquid to gas	$kg \cdot m^{-3} \cdot s^{-1}$	τ_{cond}	Time scale for heat conduction across the interface	s
Γ_{lg}^{+}	The positive part of Γ_{lg}, if $\Gamma_{lg}<0$, $\Gamma_{lg}^{+}=0$	$kg \cdot m^{-3} \cdot s^{-1}$	τ_{turb}	Time scale for turbulence eddies renewing the interface	s
Γ_{gl}^{+}	The positive part of Γ_{gl}, if $\Gamma_{gl}<0$, $\Gamma_{gl}^{+}=0$	$kg \cdot m^{-3} \cdot s^{-1}$	$\vec{\tau}_g$	Shear stress acting on the gas phase	$kg \cdot m^{-2} \cdot s^{-2}$
λ_l	Liquid thermal conductivity	$W \cdot m^{-1} \cdot K^{-1}$	$\vec{\tau}_l$	Shear stress acting on the liquid phase	$kg \cdot m^{-2} \cdot s^{-2}$
λ_t	Eddy conductivity	$W \cdot m^{-1} \cdot K^{-1}$			

REFERENCES

ANSYS, ANSYS CFX-Solver Theory Guide (2018)

Avdeev, A. A. *Bubble systems*, Springer, Berlin & Germany, 2016.

Aleksandrov, Y. A. *Bubble chambers*, Indiana University Press, Bloomington, Indiana, 1967.

Banerjee, S., et al. “Mass transfer to falling wavy liquid films in turbulent flow”, *I & EC Fundamentals*, 7, 22-27 (1968).

Birkhoff, G., et al. “Spherical bubble growth”, The Physics of Fluids, 1, 201-204 (1958)

Chen, E., et al. “Modeling of low-pressure subcooled boiling flow of water via the homogeneous MUSIG approach”, *Nuclear Engineering and Design*, 239, 1733-1743 (2009).

Ceuca, S. -C. *Computational simulations of direct contact condensation as the driving force for water hammer*, PhD thesis, Technical University of Munich, Munich & Germany, 2015

Danckwerts, P. V. “Significance of liquid-film coefficients in gas absorption”, *Industrial & Engineering Chemistry*, 43, 1460-1467 (1951).

Fan, L.T, et al. “The surface-renewal theory of interphase transport: A stochastic treatment”, *Chemical Engineering Science*, 48, 3971-3982 (1993).

Forster, H. K., Zuber, N. “Growth of a vapor bubble in a superheated liquid”, *Journal of Applied Physics*, 25, 474-478 (1954).

Florschuetz, L.W., et al. “Growth rates of free vapor bubbles in liquids at uniform superheats under normal and zero gravity conditions”, *International Journal of Heat and Mass Transfer*, 12(11), 1465-1489 (1969).

Fortescue, G. E., Pearson, J.R.A. “On gas absorption into a turbulent liquid”, *Chemical Engineering Science*, 22, 1163-1176 (1967).

Giese, T., Laurien, E. “Experimental and numerical investigation of gravity-driven pipe flow with cavitation”, *10th International Conference on Nuclear Engineering*, Arlington, VA, April 14-18, 2002.

Heinze, D., et al. “Simulation of direct contact condensation of steam jets submerged in subcooled water by means of a one-dimensional two-fluid model”, *10th International Conference on Heat Transfer, Fluid Mechanics and Thermodynamics*, Orlando, Florida, July 14-16, 2014.

Higbie, R. "The rate of absorption of a pure gas into still liquid during short periods of exposure", *Transaction of the American Institute of Chemical Engineers*, 31, 365-389, 1935.

Hughmark, G. A. “Mass and heat transfer from a rigid sphere”, *AIChE J*., 13, 1219-1221 (1967).

Janet, J. P., et al. “Heterogeneous nucleation in CFD simulation of flashing flows in converging-diverging nozzles”, *International Journal of Multiphase Flow*, 74, 106-117 (2015).

Kol'chugin, B. et al. “Study of the mechanism of cavitation in the water flow in the temperature range 125 – 250 ^{o}C”, *Heat Transfer and Hydrodynamics in Power Industry*, 123-136 (1976).

Krepper, E., et al. “On the modelling of bubbly flow in vertical pipes”, *Nuclear Engineering and Design*, 235, 597-611 (2005).

Krepper, E., et al. “The inhomogeneous MUSIG model for the simulation of polydispersed flows”, *Nuclear Engineering and Design*, 238, 1690–1702 (2008).

Krepper, E., et al. “CFD modelling of polydispersed bubbly two-phase flow around an obstacle”, *Nuclear Engineering and Design*, 239, 2372–2381 (2009).

Krepper, E., et al. “A population balance approach considering heat and mass transfer – Experiments and CFD simulations”, *Nuclear Engineering and Design*, 241, 2889–2897 (2011).

Krepper, E., et al. “CFD for subcooled flow boiling: Coupling wall boiling and population balance models”, *Nuclear Engineering and Design*, 255, 330-346 (2013).

Labuntzov, D., et al. “High speed camera investigation of bubble growth for saturated water boiling in a wide range of pressure variations”, *Thermophysics of High Temperature*, 2, 446-453(1964), in Russia.

Lakehal, D., Labois, M. “A new modelling strategy for phase-change heat transfer in turbulent interfacial two-phase flow”, *International Journal of Multiphase Flow*, 37, 627-639 (2011)

Liao, Y., et al. “Development of a generalized coalescence and breakup closure for the inhomogeneous MUSIG model”, *Nuclear Engineering and Design*, 241, 1024-1033 (2011).

Liao, Y., et al. “Flashing evaporation under different pressure levels”, *Nuclear Engineering and Design*, 265, 801-813 (2013).

Liao, Y., et al. “Application of new closure models for bubble coalescence and breakup to steam–water vertical pipe flow”, *Nuclear Engineering and Design*, 279, 126-136 (2014).

Liao, Y., et al. “Baseline closure model for dispersed bubbly flow: Bubble coalescence and breakup”, *Chemical Engineering Science*, 122, 336-349 (2015).

Liao, Y., Lucas, D. “3D CFD simulation of flashing flows in a converging-diverging nozzle”, *Nuclear Engineering and Design*, 292, 149-163 (2015).

Liao, Y., Lucas, D. “Poly-disperse simulation of condensing steam-water flow inside a large vertical pipe”, *International Journal of Thermal Sciences*, 104, 194-207 (2016).

Liao, Y., Lucas, D. “Computational modelling of flash boiling flows: A literature survey”, *International Journal of Heat and Mass Transfer*, 111, 246-265 (2017).

Liao, Y., et al. “Eulerian modeling of turbulent bubbly flow based on a baseline closure concept”, *Nuclear Engineering and Design, 337, 450-459* (2018a).

Liao, Y., Lucas, D. “Evaluation of interfacial heat transfer models for flashing flow with two-fluid CFD”, *Fluids 2018*, 3, 38; doi:10.3390/fluids3020038 (2018b).

Liao, Y., et al. “Application of a novel model for bubble-induced turbulence to bubbly flows in containers and vertical pipes”, *Chemical Engineering Science*, 2019, https://doi.org/10.1016/j.ces.2019.03.007

Lucas, D. et al. “A Strategy for the qualification of multi-fluid approaches for nuclear reactor safety”, *Nuclear Engineering and Design*, 299, 2-11 (2016).

Lutovinov, S. Z. *Investigation of hot water discharge at tube rupture in application to the accident situation at nuclear power plant*, Ph.D. thesis; Krzhizhanovsky Power Engineering Institute; Moscow; 1985.

Ma, T., et al. “Direct numerical simulation-based Reynolds-averaged closure for bubble-induced turbulence,” *Physical Review Fluids* 2, pp. 034301/1-034301/11 (2017).

Mahaffy J, et al. “Best practice guidelines for the use of CFD in nuclear reactor safety applications”, Organisation for Economic Co-Operation and Development, 2007.

Maksic, S., Mewes, D. “CFD-calculation of the flashing flow in pipes and nozzles”, *ASME 2002 Fluids Engineering Division Summer Meeting*, Montreal, Quebec, Canada, July 14-18, 2002.

Marsh, C., Withers, D. “CFD modelling of direct contact steam injection”, *5th International Conference on CFD in the Process Industries CSIRO*, Melbourne, Australia, December 13-15, 2006

Mathpati, C. S., Joshi, J. B. “Insight into theories of heat and mass transfer at the solid-fluid interface using direct numerical simulation and large eddy simulation”, *Industrial & Engineering Chemistry Research*, 46, 8525-8557 (2007).

Morsi, B. I., Basha, O. M. *Mass transfer in multiphase systems, mass transfer - advancement in process modelling*, Dr. Marek Solecki (Ed.), InTech, DOI: 10.5772/60516. Available from:https://www.intechopen.com/books/mass-transfer-advancement-in-process-modelling/mass-transfer-in-multiphase-systems, 2015

Murallidharan, J. S., et al. “CFD investigation and assessment of wall heat flux partitioning model for the prediction of high pressure subcooled flow boiling”, *International Journal of Heat and Mass Transfer*, 103, 211-230 (2016).

Perlmutter, D.D. “Surface-renewal models in mass transfer”, *Chemical Engineering Science*, 16, pp. 287-296 (1961).

Plesset, M. S., Zwick, S. A. “The growth of vapor bubbles in superheated liquids”, *Journal of Applied Physics*, 25, 493-500 (1954).

Ranz, W. E., Marshall, Jr., W. R. “Evaporation from drops, Part II”, *Chemical Engineering Progress*, 48(4), 173–180(1952).

Ruckenstein, E., Davis, E. J. “The effects of bubble translation on vapor bubble growth in a superheated liquid”, *International Journal of Heat and Mass Transfer*, 14, 939-952 (1971).

Scheuerer, M. et al. “Evaluation of computational fluid dynamic methods for reactor safety analysis (ECORA)”, *Nuclear Engineering and Design*, 235, 359-368(2005).

Shah, A. et al. “Numerical simulation of direct-contact condensation from a supersonic steam jet in subcooled water”, *Fluid Flow and Transport Phenomena, Chinese Journal of Chemical Engineering*, 18, 577-587 (2010).

Tomiyama, A., et al. “Transverse migration of single bubbles in simple shear flows,” *Chemical Engineering Science*, 57, 1849–1858 (2002).

Tomiyama, A. “Progress in computational bubble dynamics”, *Workshop on Multiphase Flow*, Dresden, Germany, May 27, 2009.

Walton, D.E. “The evaporation of water droplets: a single droplet drying experiment”, *Drying Technology*, 22, 431-456 (2004).

Wellek, R.M., et al. “Shape of liquid drops moving in liquid media”, *AIChE Journal*, 12, 854-862 (1966).

Whitaker, S. “Forced convection heat transfer correlations for flow in pipes, past flat plates, single cylinders, single spheres, and for flow in packed beds and tube bundles”, *AIChE Journal*, 18(2), 361-371(1972).

Wolfert, K., et al. “Non-equilibrium mass transfer between liquid and vapour phases during depressurization process in transient two-phase flow”, *In: Proc. 2nd CSNI Specialists Meeting*, Paris, 1978

Yang, L., et al. “Computational fluid dynamics simulation of subcooled flow boiling in vertical rectangular 2-mm narrow channel”, *Advances in Mechanical Engineering*, 7, 1-12 (2015).

Yeoh, G.H. et al. „On the prediction oft he phase distribution of bubbly flow in a horizontal pipe”, *Chemical Engineering Research and Design*, 90, 40-51 (2012).

Zhang, R., et al. “Effects of turbulence models on forced convection subcooled boiling in vertical pipe”, *Annals of Nuclear Energy*, 80, 293-302 (2015).